5

Small Wind Turbine Technology

Oliver Probst[1], Jaime Martínez[1,2], Jorge Elizondo[1,2] and Oswaldo Monroy[1]
[1]*Instituto Tecnológico y de Estudios Superiores de Monterrey, Monterrey*
[2]*Diseño Eólico y Solar, Monterrey*
Mexico

1. Introduction

Small wind turbines are an attractive alternative for off-grid electrification and water pumping, both as stand-alone applications and in combination with other energy technologies such as photovoltaic, small hydro or Diesel engines. Under these conditions, the cost of energy alone is often not the only criterion to consider, and aspects like system performance, suitability for a given wind regime, reliability under normal and extreme wind conditions, and overall system life are often equally important. Where no grid connection is available or the grid is unreliable, it is the energy-providing service that matters, not its precise cost. In grid-connected situations, the actual vs. the rated performance may be of more interest in order to achieve the cost saving benefits proposed in the design of the project. In either case, an uninterrupted service with a performance close to the one specified by the provider is a key requirement for a successful small wind project.

While all wind turbines, both MW-class utility turbines and small wind generators, are subject to the fluctuating nature of the wind, there are several reasons why it is more difficult to guarantee the performance of a small wind turbine. First, the smaller inertia of rotor/generator leads to significant transient effects in response to changing wind speeds. Moreover, often small wind turbines rely on passive mechanisms for aligning the rotor with the wind direction, such as lifting forces acting on a tail vane in the case of an upwind rotor or axial (drag and lift) forces acting on the rotor in the case of a downwind turbine. Therefore, under conditions of varying wind directions, an incomplete alignment of wind turbine and wind direction may occur, and the alignment error can be expected to be a function of the turbulent time scales present at the site. In the case of furling systems, a technology used by many manufacturers to passively protect the turbine from overspeeding and generator overheating, the situation is still far more complex since the mechanism can be triggered both by sustained high winds and gusts, also exhibiting a hysteresis depending on the specific design parameters chosen.

Another important aspect relates to maintenance. While large wind turbines are routinely serviced as part of an ongoing service agreement during the lifetime of a wind farm and are constantly monitored by means of a SCADA (supervisory control and data acquisition) system, small wind generators are expected to function largely unsupervised and with only occasional maintenance. Therefore, the only indication for a typical owner of a small wind turbine is the charge level of the battery, which is only very indirectly related to the (integrated) wind turbine system performance in the period prior to the observation.

Systematic measurement campaigns are therefore essential to assess the system performance under quasi-steady state conditions and compare this performance to the predictions of the theoretical design model, study the turbine under transient conditions, such as during furling and start-up, and detect energy losses due to storage or inappropriate matching of turbine capacity and battery size, among others. All these issues will be addressed in the present chapter.
Another issue yet has to do with the very concept of performance certification and verification. While large wind turbines are often certified according to international standards, generally the IEC61400-12, only recently a performance standard for small wind turbines has been issued (AWEA 2009). While certification may be a high financial burden, especially for small companies with a modest output of units, a unit-by-unit on-site performance verification is generally prohibitive because of the cost and complexity of the associated measurement equipment. More importantly still, due to the generally low output voltage level Joule losses on the transmission line from the hub height to the battery bank, end-use application or grid-intertie inverter significantly impact on the true amount of energy captured. Small wind turbine providers therefore often specify the expected power or energy output at the nacelle, i.e. before the transmission line. While this is a sound practice, the end user has to be aware of the fact that the true energy output may be substantially less than announced. This and related issues will be addressed in the chapter.

2. Conceptual design of small wind turbine systems

While no strict definition of a small wind turbine exists in literature, wind turbines with a rated capacity of 10kW or less are generally considered *small*; this definition is sometimes extended up to about 50kW due to the recent appearance of higher rated machines suitable for servicing more energy demanding applications, including agricultural tasks such as water pumping for irrigation or livestock watering. As it will explained below, rated capacity is not a very well defined parameter for a small wind turbine, so the rotor diameter or, equivalently, the swept rotor area are often preferred for classifying small wind turbines, where rotor diameters of about 10m can be taken as the dividing line. Another means of distinguishing *small* from *large* wind turbines is by requiring a small wind turbine to have a tail vane (see discussion below). While in principle many of the aspects discussed in this chapter can be applied to vertical- and horizontal-axis wind turbines equally we will limit ourselves to the latter only.
A small wind turbine generally consists of the following minimal components: (1) A rotor with a variable number of blades (section 3), (2) an electric generator (section 4), and (3) passive or active electronic components (section 6) for feeding electricity into a battery bank, the public grid or, occasionally, into a direct application such as a water-pump. Upwind wind turbines are generally equipped with a tail vane to assure the rotor is facing the wind, while downwind turbines rely on the self-orienting effect of the axial forces acting on the rotor, albeit at the expense of a periodic tower shading effect acting on the turbine blades. Many upwind turbines rely on a furling mechanism for overspeed and output power control at high wind speeds, although other mechanisms such as load-induced stall are used occasionally. Passively pitching blades, generally triggered by the action of the centrifugal forces acting on the rotor, have been used in the past but are currently less common.
Most small wind turbines are variable-frequency devices, allowing for an optimal operation at all wind speeds below the threshold for the onset of the overspeed and power control

mechanism. While in the case of battery-charging applications the use of a passive rectifier together with the selection of an appropriate voltage level may be sufficient to maintain the operating point close to the system optimum, especially when the aerodynamic efficiency curve (section 6) is broad (Elizondo et al., 2009, Probst et al., 2006), some commercial systems rely on the use of an active load control in order to maintain the system at the optimal operating point for each wind speed (Martínez et al., 2006). In the case of a coupling to the electric grid, a full *wild* AC/fixed frequency AC conversion is generally feasible through the use of a *back-to-back* AC/DC/AC converter, as opposed to large wind turbines where a direct full conversion is still rather the exception than the rule and most commercial large wind turbines rely on doubly fed induction generators (DFIG) where only a fraction of the total power is passed through a converter.

3. Rotor aerodynamics and loads

Just like large wind turbines most modern small wind turbines use a three-bladed rotor with aerodynamic sections (airfoils), although designs with two or four blades are occasionally encountered. Two-bladed rotors develop their optimal aerodynamic performance at higher tip speed ratios (TSR) and therefore have to rotate faster than three-bladed rotors. This allows for the use of high-speed electric generators which are smaller and less expensive to manufacture, although at the expense of potentially greater noise problems. Multi-bladed rotors, on the other hand, have a higher starting torque which favors starting at low wind speeds.

Due to the smaller dimensions, the Reynolds numbers (Re) at sections of small wind turbine blades are considerably smaller than for large wind turbine blades. While typical Reynolds numbers for large wind turbines are in excess of 10^6, where the aerodynamic lift and drag coefficients vary little with Re, at small wind turbine blades the aerodynamic performance of a given airfoil may be substantially poorer at the inboard sections, where the Reynolds number may be of the order of 100,000 or less. Low Reynolds number operation is highly dependent on the behavior of the laminar boundary layer (Selig and McGranahan, 2004), so ambient turbulence and surface roughness have a pronounced effect on the wind turbine behavior. Surface roughness is generally affected by the manufacturing technique, but may also change considerably over time due to soiling. In Fig. 1 two examples illustrating the effect of soiling are shown for two airfoils (the E387 and the S822) designed for the use with small wind turbines (data from Selig and McGranahan, 2004). In their experiments, Selig and McGranahan simulated the effect of airfoil soiling by attaching a zigzag shaped boundary layer trip to the airfoil surface.

In the graphs, the ratio between the lift and the drag coefficient has been plotted as a function of the angle of attack for both clean and soiled surfaces. It is conspicuous from the figure that lift/drag quotient is substantially reduced in the angle-of-attack range in which the rotating airfoils will be operating most of the time. The maximum C_L/C_D value is reduced from 80 to about 55 in the case of the E387 airfoil and from 65 to 40, a 31% and 38% reduction, respectively. Also, the difference in aerodynamic performance between attached flow and stall conditions is decreased since the performance in stall is little affected by soiling, so the effectiveness of turbine power control schemes based on active stall regulation, either by load control or by pitching the blades towards higher angles of attack, is greatly reduced if soiling is not controlled.

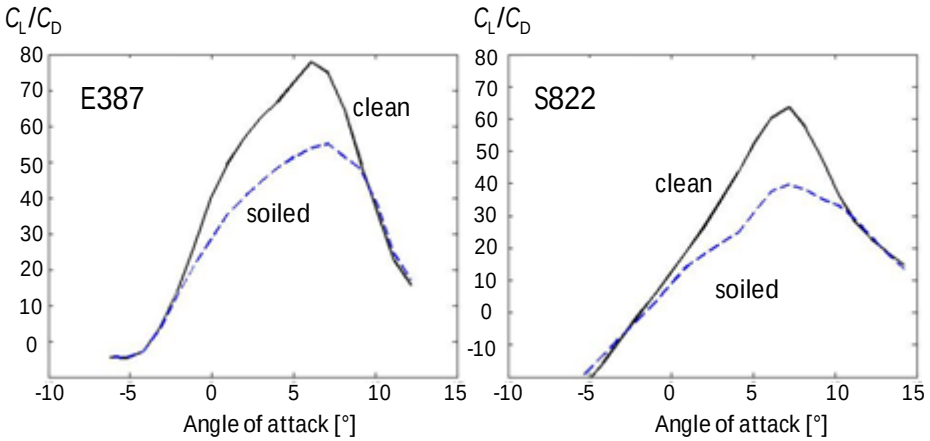

Fig. 1. Effect of airfoil soiling on the ratio of lift and drag coefficient for two airfoils designed for small wind turbines (Reynolds number=100,000). Data from Selig and McGranahan (2004)

A characteristic element of low Reynolds number flow is the appearance of a laminar separation bubble caused by the separation of the laminar flow from the airfoil with a subsequent turbulent reattachment (Selig and McGranahan, 2004). This phenomenon leads to a considerable increase in the drag coefficient at low angle of attack. This quite dramatic drag increase is illustrated in Fig. 2 where the measured C_L-C_D diagram (drag polars) for the Eppler airfoil E387 (data from Selig and McGranahan, 2004) has been drawn for Reynolds numbers in the 100,000 to 500,000 range. While a moderate increase in drag occurs for any given lift coefficient upon decreasing the Reynolds number from 500,000 to 200,000, the drag at 100,000 is substantially higher.

Low Reynolds number flow also has higher associated uncertainties, as shown by Selig and McGranahan (2004, chapter 3) in their comparisons of their aerodynamic force measurements with those obtained at the NASA Langley in the Low-Turbulence Pressure Tunnel (McGhee et al., 1988). While an excellent agreement between the two sets of measured drag polars is obtained for Reynolds numbers of 200,000 and higher, substantial differences arise at 100,000. Although the same shape of the drag polars was observed in both cases, showing the appearance of the laminar separation bubble, the drag coefficients for a given lift coefficient were found to be higher in the measurements by Selig and McGranahan (2004). Interestingly, a similar discrepancy, limited to the low Reynolds number case of 100,000, was found in a theoretical analysis of small-scale wind turbine airfoils (Somers and Maughmer, 2003), including the Eppler airfoil E387 mentioned above. In their study, the authors use two different airfoil codes, the XFoil and the Eppler Airfoil Design and Analysis Code (Profil00), finding similar results for drag polars, except for the low Reynolds number case of 100,000, where the experimentally observed drag is better reproduced by the Profil00 code. From the above it should have become clear that the uncertainty in the prediction of the lift and drag coefficients at low Reynolds is larger than at higher Reynolds, making predictions of rotor performance and energy yield less accurate.

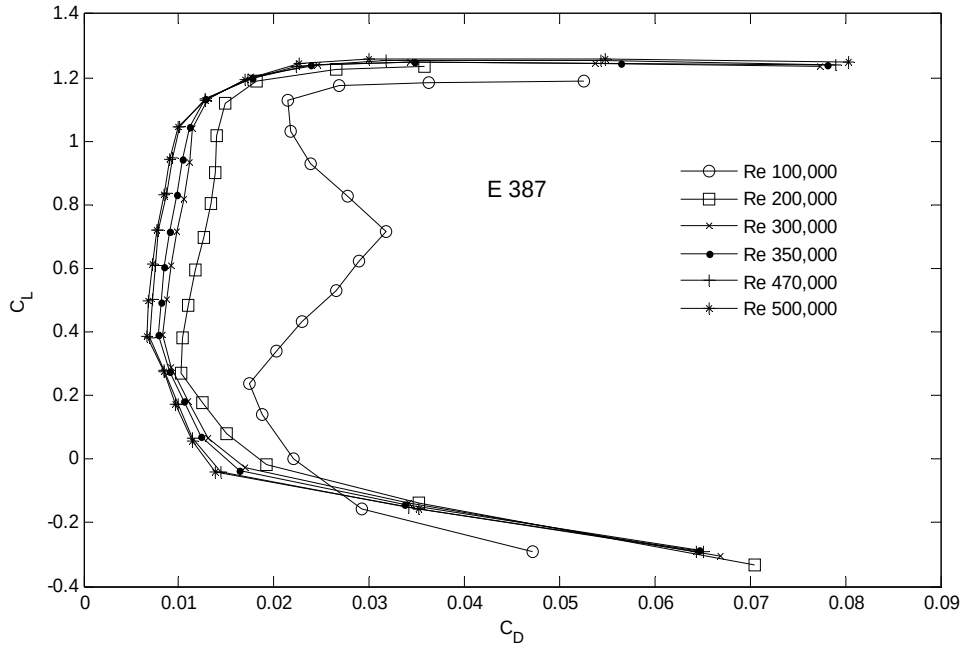

Fig. 2. Aerodynamic lift vs. drag coefficient for the Eppler airfoil E387 designed for the use with small-scale wind turbines. After Selig and McGranahan (2004)

A direct consequence of the lower aerodynamic performance at low Reynolds numbers is a generally somewhat lower aerodynamic power coefficient (C_p< 0.46-0.48 for a well-designed rotor at peak efficiency, as opposed to >0.50 for large wind turbines) and a dependence of C_p on both the tip speed ratio (TSR) and the wind speed, as opposed to large rotors, where to a good approximation the power coefficient is a function of TSR only. This effect is illustrated in Fig. 3, where the experimental results of the aerodynamic power coefficient C_p vs. the tip speed ratio (TSR) λ of a turbine rated at 1.4 kW (swept diameter 3m), obtained from a field characterization, have been plotted together with the predictions of a mathematical model of the turbine. The experimental data was obtained by operating the turbine under different controlled load conditions, including direct connection to a battery bank with a voltage of 48V, 24V, or 12V; to provide higher load conditions, the 12V battery bank was shunted with a resistance whose value was varied from 2.1Ω to 1.1Ω (Elizondo et al., 2009). It can be seen that for low values of the tip speed ratio all power coefficient values fall onto a universal curve, while for higher TSR values a greater spread between the recorded values exsist, as predicted by the mathematical model based on a combination of a Blade Element Momentum (BEM) and an electromechanical model of the generator/rectifier. The appearance of different C_p - λ curves at high values of TSR can be traced back to the lower aerodynamic performance of the blade sections at low wind speeds (and therefore low Reynolds numbers), as illustrated by the difference of the lower curve in Fig. 3 (corresponding to a wind speed of 6 m/s) and the higher curve (valid for 12 m/s).

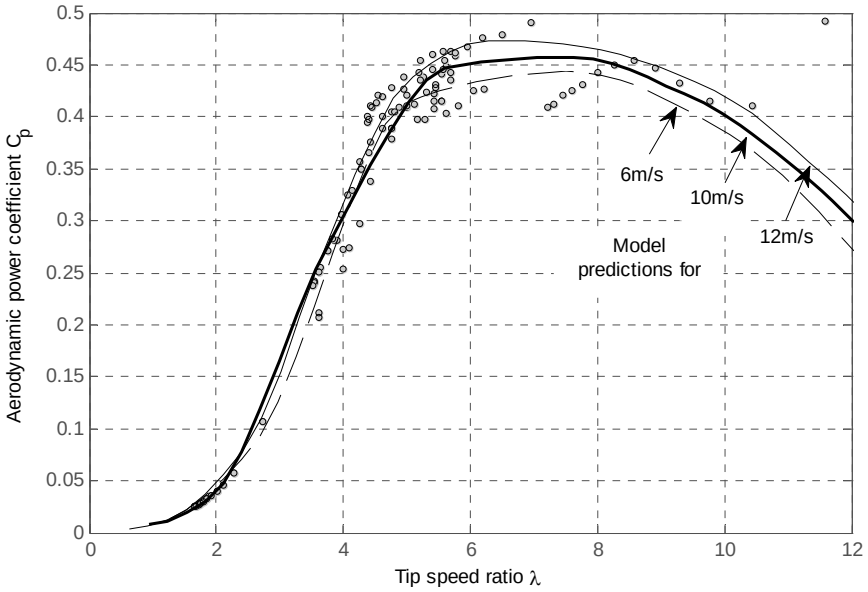

Fig. 3. Measured C_p-λ curve for a wind turbine rated at 1.4 kW and comparison with the predictions of a mathematical model of the turbine.

Another important point refers to the influence of the average blade aspect ratio; while long slender blades can be often well described with Blade Element Momentum (BEM) models using aerodynamic lift and drag coefficients determined in the wind tunnel under two-dimensional flow conditions, three-dimensional effects become important for blades with low aspect ratios, especially under conditions of flow separation or *stall*. As shown by Martínez et al. (2005), a good prediction (as opposed to a parametric fit) of the output power curves was obtained by modeling several research wind turbines with rated capacities in the range of 10-20kW by combining a 2D with a 3D-stall model. For that purpose, the lift coefficient as a function of the angle of attack of a given blade section was modeled according to

$$C_{L,\text{eff}} = \begin{cases} C_{L,\text{wind tunnel}}(\alpha) & \alpha \le \alpha_S \\ \frac{1}{2}\left(C_{L,\text{VC}}(\alpha;\kappa=50) + C_{L,\text{VC}}(\alpha;\kappa=\kappa_0)\right) & \alpha > \alpha_S \end{cases} \tag{1}$$

where $C_{\text{L,wind tunnel}}$ refers to the lift coefficient of the blade section measured under 2D flow conditions, and $C_{\text{L,VC}}$ is the lift coefficient as determined by the Viterna-Corregan stall model (Martínez et al., 2005):

$$C_L = \tfrac{1}{2} C_{D,\max} \sin 2\alpha + K_L \cos^2\alpha / \sin\alpha \tag{2}$$

$$C_D = C_{D,\max} \sin^2\alpha + K_D \cos\alpha \,, \tag{3}$$

where

$$K_L = \left(C_{L,S} - C_{D,\max} \sin\alpha_S \cos\alpha_S\right) \sin\alpha_S \Big/ \cos^2\alpha_S \tag{4}$$

$$K_D = \left(C_{D,S} - C_{D,\max} \sin^2\alpha_S\right) \Big/ \cos\alpha_S \tag{5}$$

Here, $C_{L,S}$ and $C_{D,S}$ denote the lift and drag coefficient at the stall angle α_s, respectively, and $C_{D,\max}$ is the maximum drag coefficient (at α=90°). It depends on aspect ratio (defined as the ratio of the blade span L and the mean chord of the blade) as follows:

$$C_{D,\max} = \begin{cases} 1.11 + 0.018\kappa & \kappa \le 50 \\ 2.01 & \kappa > 50 \end{cases} \tag{6}$$

Another important difference between large and small wind turbines has to do with hub height. Small wind turbines are usually placed at heights around 20 to 30 meters, as compared to 60 to 80 meters for utility-scale units. Therefore, small wind turbines usually operate at wind with higher turbulence intensity on its blades, as shown in the following approximate expression (Burton et al., 2001) for the turbulence intensity TI, defined as the ratio of the standard deviation σ_u of the fluctuations of longitudinal component of the wind velocity and the wind speed U:

$$\mathrm{TI} \equiv \frac{\sigma_u}{U} = \frac{2.4u^*}{U(z)} \approx \frac{1}{\ln(z/z_0)} \tag{7}$$

where z_0 is roughness length of the site and u^* is the friction velocity. For a typical utility-scale wind turbine with a hub height of z=80m and a roughness length of 0.1m, the turbulence intensity is about 15%, whereas for a small wind turbine hub height, say, z=20m, the corresponding figure is 19%

Increased turbulent intensity has a predominantly detrimental effect on turbine performance, mostly due to increased transient behavior, causing frequent acceleration and deceleration events, increased yawing movement and vibrations on most components. Wind shear, on the other hand, can generally be neglected due to the small dimensions of the rotor.

Although structural aspects cannot be neglected in the design process of small rotor blades, their impact on the design is less pronounced compared to the large wind turbine case. Structural properties are generally analyzed after the aerodynamic design stage has been completed, as opposed to large wind turbines where the structural design precedes the aerodynamic design. In the following we will discuss the main aspects to be considered in the structural design of small-scale rotors.

Three types of main operational loads can be distinguished: (1) Inertial, (2) aerodynamic, and (3) gravitational loads. Loads on small wind turbines blades are the same as on blades of utility size wind turbines, but their relative importance is different. If we assume the tip speed ratio (λ) to be constant, the three principal forces on the blades scale can be discussed as follows: The centrifugal force on the blade root (Fig. 4) can be calculated from

$$F_c = \omega^2 \rho A \int_0^R r \, \mathrm{d}r = \tfrac{1}{2}\omega^2 \rho A R^2 \tag{8}$$

where A is the cross-sectional area of the blade. We then have

$$A \propto c \times \gamma \propto R^2 , \tag{9}$$

with c and γ being a typical chord and thickness dimension, respectively, each of which scale approximately with the blade radius R. Introducing the tip speed ratio λ by setting $\omega = \lambda U / R$ we see that the centrifugal force at the blade root scales with the square of the blade length:

$$F_c \propto R^2 . \tag{10}$$

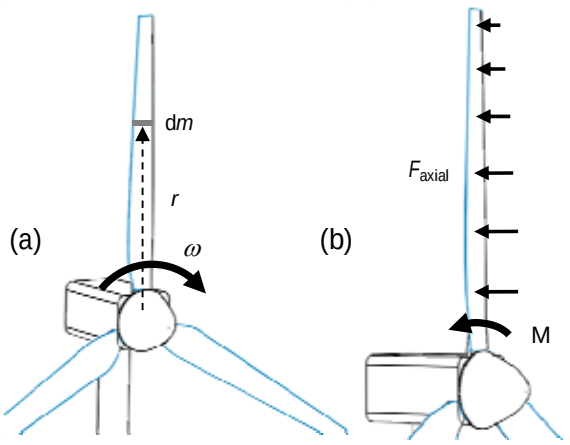

Fig. 4. Forces on a wind turbine rotor. (a) Centrifugal force on the blade root. (b) Axial force and root moment.

The aerodynamic forces create an axial load which translates into a root bending moment:

$$M = \int_0^R \mathrm{d}F_{ax}(r)\, r \quad \propto \int_0^R c\, W^2\, r\, \mathrm{d}r \tag{11}$$

where r is the distance from the rotational axis. The precise axial force variation along the blade has to be calculated through numeric methods such as Blade Element Momentum Theory. However, supposing that aerodynamic performance is not affected by the blade length (i.e. supposing the same C_L and C_D for any blade length), we know that the axial force is proportional to chord c and effective velocity W squared, as expressed in equation (11). We observe that the effective wind speed squared can be calculated from

$$W^2 = U^2 \left((1-a)^2 + \left(\lambda \frac{r}{R} \right)^2 (1+a')^2 \right) \propto \left(\lambda \frac{r}{R} \right)^2 \quad \text{for } \lambda \frac{r}{R} >> 1 \tag{12}$$

Where a, a' are the axial and tangential induction factors, respectively, and are assumed to be independent of the scaling process, i.e. are assumed equal for small and large wind turbines. It should be noted that the approximate proportionality in equation (13) is valid at most radial positions, except for the blade root. Therefore, if the tip speed ratio λ is taken to be unchanged upon scaling the blade length, then

$$M \propto R^3 \tag{13}$$

Gravitation, finally, gives rise to an oscillating force on the blade that acts alternatively as compressive, tensile or shear force, depending on the azimuthal blade position. Its magnitude depends directly on blade total mass:

$$F_g = mg = \rho g V \propto \rho g\left(c \times t \times R\right) \tag{14}$$

If we assume again that the chord c and wall thickness t scale linearly with the blade radius, then

$$F_g \propto R^3 \tag{15}$$

i.e., the gravitational force scales as the cube of the blade radius. It has been proposed in literature (Burton et al., 2001) that blade mass can be scaled as $R^{2.38}$ with a proper engineering design to optimize blade material. In either case, the axial force bending moment and gravitational force become dominant as the blade gets larger, while with small wind turbines centrifugal forces usually dominate. A direct effect of the dominant role of centrifugal forces at small blades is that blades have greater stiffness (due to centrifugal stiffening) and are only lightly bent due by the axial force.

The discussion above directly translates into guidelines for the materials selection and the manufacturing process. While mechanical properties are highly dependent on the materials used in the manufacturing process, a typical blade material is glass fiber reinforced plastic (GFRP), although wood (either as the blade material or for interior reinforcement) and carbon fiber are also used by some manufacturers. With GFRP, manufacturing methods vary widely from hand lay-up to pultrusion (e.g. Bergey), depending on whether the precise blade geometry or a high production volume are the major concern.

The observed mechanical properties for blades are usually lower than the expected properties for the material, usually due to the following causes:

a. Air bubbles can form inside the material, concentrating stress and reducing overall resistance. This is a typical situation in hand lay-up manufacturing processes.
b. Material degradation due to weathering in operating blades. Usually UV radiation and water brake polymer chains, while wind acts as an abrasive on the surface. (Kutz, 2005).
c. In small wind turbines both centrifugal and axial forces can lead to failure in the following way: Centrifugal force failures occur as a direct consequence of surpassing the tensile strength of the reinforcement and usually occur near the root where centrifugal force is maximum, and close to the bolts fixing the blade due to stress concentration. Failures due to axial force bending moments usually occur due to buckling in the inboard section of the blade.

4. Generators

The generator is the center piece of a small wind turbine. The advent of powerful permanent magnets based on Neodymium has opened the door to compact permanent magnet synchronous generator designs (Khan et al., 2005) with potentially high efficiencies. Radial flow generators are still the predominant choice, but axial flow designs (Probst et al., 2006) are becoming increasingly popular because of their modular design and relatively low

manufacturing requirements. Currently, axial flow designs are typically limited to smaller-scale turbines with rated capacities of 10 kW or less due to the strong increase in structural material requirements for larger machines. Induction generators are occasionally used because of the abundance and low cost of induction machines which can be configured as generators, but are suitable only for grid-coupled applications.
Designing an efficient generator requires an understanding of the different loss mechanisms prevailing in such generators. Often, Joule losses occurring at the armature winding of the stator coils (often referred to as *copper losses*) are by far the greatest source of losses, so care has to be taken to avoid overheating, either by using high-voltage designs, allow for a large wire cross section to reduce armature resistance, provide efficient passive cooling mechanisms, or a combination of the former. Clearly, higher magnetic field strengths lead to higher induction voltages which in turns allow for lower currents, hence the need for powerful magnets. Iron cores instead of air cores can be used to increase the magnetic flow and therefore the induction voltage, albeit at the expense of a cogging torque (detrimental at startup) and higher stator inductivity (Probst et al., 2006). Wiring several stator coils in series is often a simple and efficient measure to increase the system voltage and diminish copper losses. Peak efficiencies of about 90% can be achieved with such a scheme even in a modest manufacturing environment (Probst et al., 2006). Under more stringent manufacturing conditions, where a small and stable air gap between the stator and the rotor can be assured, efficiencies of the order of 95% can be achieved routinely (Khan et al., 2005).

4.1 Common generator topologies

As described above, the electric generators of modern small wind turbines are generally designed to use permanent magnets and a direct coupling between rotor and generator. The following common topologies can be encountered:

1. Axial flow air-cored generators
2. Axial flow generators with toroidal iron cores
3. Axial flow generators with iron cores and slots
4. Radial flow generators with iron cores and slots
5. Transverse flow generators with slotted iron core

In the topologies above the type of flow refers to the direction of the magnetic flow lines crossing the magnetic gap between the poles with respect to the rotating shaft of the generator. Once the flow lines reach the iron core (in practical realizations actually laminated steel), the flow lines may change their direction according to the geometry of the core. Two of the most common topologies are shown in Fig. 5 and Fig. 6, respectively. Fig. 5 shows a typical radial magnetic flow topology, whereas Fig. 6 exhibits the conceptual design and magnetic flow field of an axial flow generator. Similar magnetic flux densities can be achieved in the magnetic gap for both topologies, but the axial flow geometry has the advantage of a modular design, since the two rotor disks and the stator disk (not shown) can be simply stacked on the rotor axis, making this design conceptually attractive for small-scale wind turbines, where often less sophisticated manufacturing tools are available than for large wind turbines.
Each topology has specific advantages and disadvantages (Dubois et al., 2000; Yicheng Chen et al., 2004; Bang et al., 2000), which makes it difficult to define a clearly preferred choice; in most cases the topology chosen will depend on the design preference. An overview of the most important up- and downsides is given in Table 1.

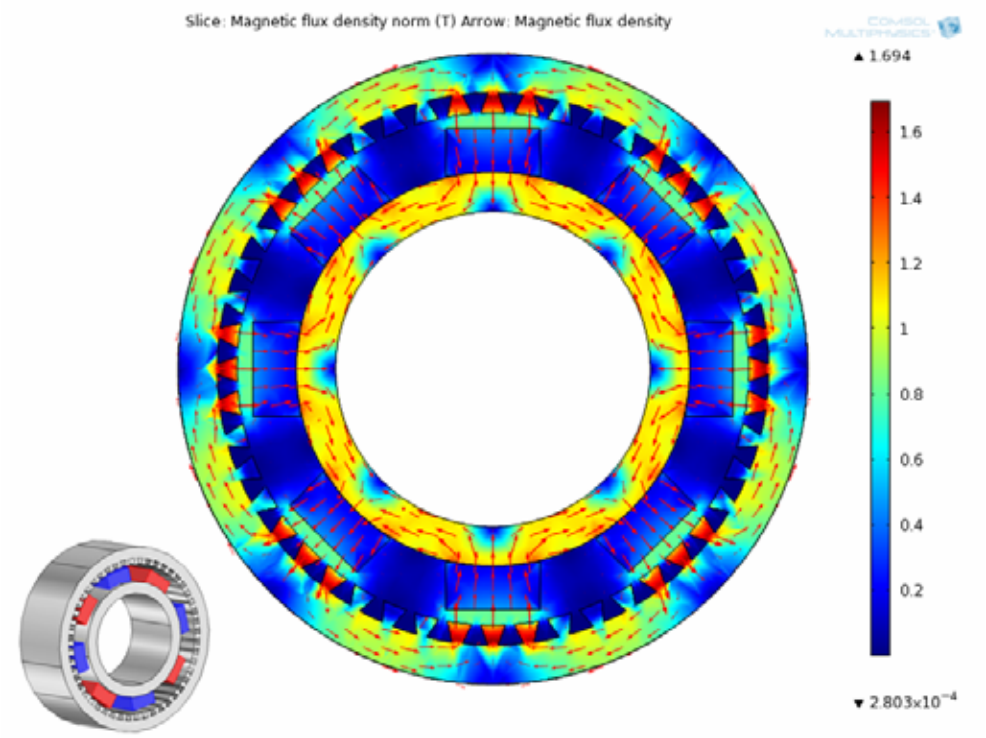

Fig. 5. Typical radial flow permanent magnet generator with iron core and slots. Small figure: Perspective view of general arrangement. Main figure: Color map: Magnetic flux density in T. Arrows: Magnetic flux density vector field.

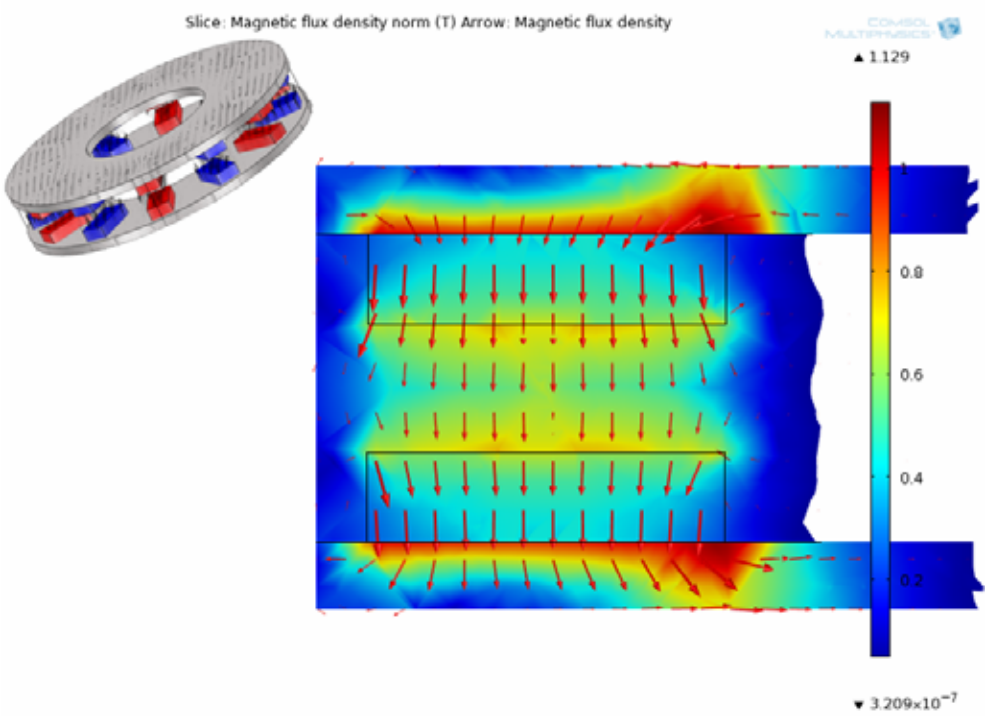

Fig. 6. Typical axial flow permanent magnet generator with iron core. Small figure: Perspective view of general arrangement. Main figure: Color map: Magnetic flux density in T. Arrows: Magnetic flux density vector field.

Topology	Advantages	Disadvantages
Axial flow with air core	Simple design and manufacture No cogging torque Quiet operation Low risk of demagnetization of permanent magnets No core losses Stackable and therefore scalable generators Multi-phase operation can be implemented easily	Structural challenges for maintaining a constant air gap for larger diameters Possible thermal instability of the polymer resin encapsulation Large amount of neodymium required Large external diameter Eddy losses in copper windings
Axial flow with toroidal iron core	Simple design and manufacture No cogging torque Quiet operation Low risk of demagnetization of permanent magnets No core losses Stackable and therefore scalable generators Multi-phase operation can be implemented easily Short end-coil connections	Structural challenges for maintaining a constant air gap for larger diameters Large amount of neodymium required Large external diameter Eddy losses in copper windings and in iron core
Axial flow with iron core and slots	Very high torque density Stackable and therefore scalable generators	Structural challenges for maintaining a constant air gap for larger diameters Complex manufacture Presence of cogging torque Relatively noisy Eddy core losses
Radial flow with iron core and slots	Structurally more robust tan axial flow generators; therefore less structural material required More widely used and well-known topology Smaller exterior diameter Diameter can be defined without considering the axial length	Presence of cogging torque Relatively noisy Eddy core losses Large amount of magnetic material due to laminated core.
Transverse flow with slots in iron core	Generally needs the least amount of neodymium Low copper losses Simple coil winding High torque density, if properly designed	Complex design and manufacture Uncommon topology so far Potentially high magnetic dispersion Potentially low power factor Presence of cogging torque Needs a stator for each electric phase Eddy core losses

Table 1. Comparative table of different generator topologies commonly used in small-scale wind turbines

4.2 Mechanical loads

Independently of the generator topology chosen, a structural analysis is indispensable before settling on a specific generator design. In small wind turbines it is common to directly couple the rotor and the generator; therefore mechanical loads on the rotor are directly transferred to the generator. Several extreme conditions should be considered when evaluating a generator design:

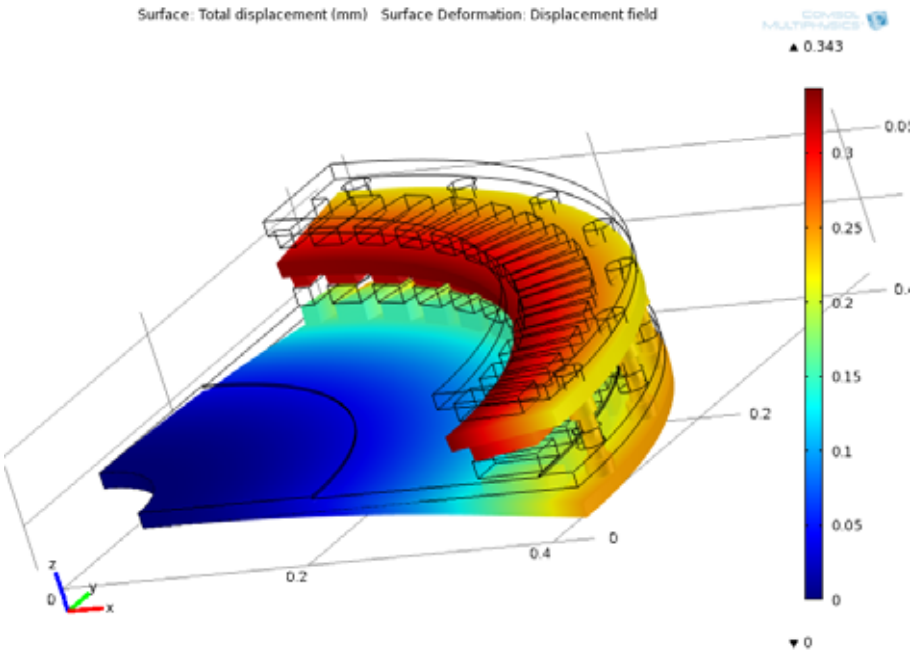

Fig. 7. Axial displacement field for the deformation of the rotor disks of an axial flow permanent magnet generator due to magnetic forces between the magnets

Electromagnetic forces. Since Neodymium magnets are particularly strong, their forces on the structural design have to be considered carefully. These forces are especially important for axial flow designs where either the axial forces between the magnets and the iron core or the forces between magnets (in the case of air cores) have to be considered. A common consequence is a deformation of the rotating disks on which the magnets are mounted, thereby reducing the clearance between stator and rotational disks. This reduction affects the magnetic flow distribution at best, but can ultimately lead to a collision between the disks and therefore the destruction of the generator, if not properly accounted for. Fig. 7 shows an example of the axial deformation field simulated for an axial flow permanent magnet generator with a free gap between the magnets and toroidal stator (not shown) of 3mm. Independent assessments determined that the tolerance of gap width should not be larger than 5% of this value, i.e. 0.15mm. For the design shown in Fig. 7, however, where the separation of the rotor plates is controlled by a ring of bolts distributed at the outer perimeter of the disks, axial displacements over 0.3mm are observed at the inner perimeter, leading to a considerable reduction in free gap width.

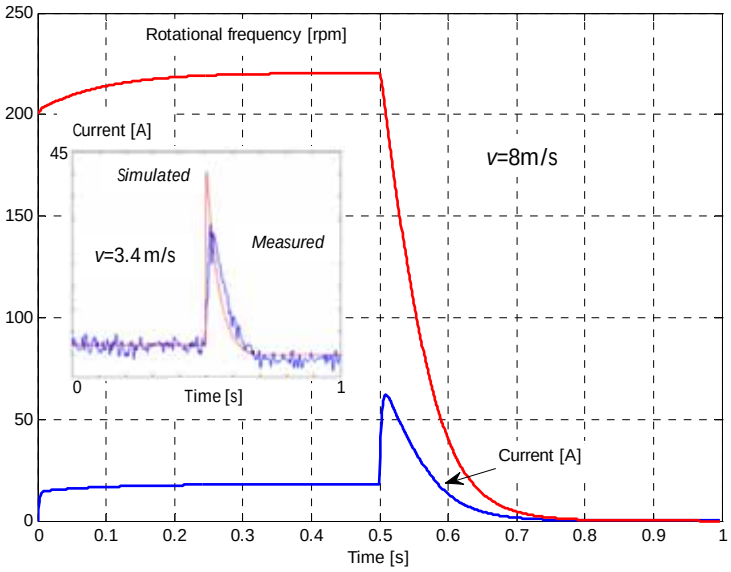

Fig. 8. Simulation of a short-circuit event. *Main figure*: Rotational frequency and stator current as a function of time. The short-circuit occurs at 0.5s. The wind speed was taken as 8 m/s. *Inset:* Simulated vs. measured stator current for a wind speed of 3.4 m/s.

Abrupt braking. It is important to consider different failure modes, such as the occurrence of a continuous short circuit at the generator terminals. This kind of failure leads to an abrupt braking of the rotor and may cause severe damage if not contemplated at the mechanical design stage. In the first place, excessive mechanical stress may occur at the structural elements due to the high braking torque. Moreover, thermal stress may occur due to the high electric current flowing under the short-circuit conditions, which is only limited by the internal resistance and inductance of the stator coils. Overheating occurring under these conditions may damage the wiring of the stator and electronic components. En Fig. 8 a simulation of the effect of such a short-circuit event is shown for the variables rotor frequency and stator current (main figure, wind speed = 8 m/s). In the inset of the figure, an example of the validation of the dynamic model is given for a wind speed of 3.4 m/s. In either case it can be observed that upon short-circuiting the rotor a steep rise in stator current is obtained, followed by a slower decay once the rotor-generator slows down as the result of the strong opposing torque. It is conspicuous from Fig. 8 that the rotation is brought to a complete halt in less than 0.2 seconds, after an initial condition of about 225rpm, with most of the braking occurring during the first 0.1 seconds. Such a spike both in mechanical torque and in current creates strong mechanical and thermal stresses, respectively, and can inflict severe damage to the rotor-generator (including the complete destruction), if not accounted for properly.

Blade fracture. Small-scale wind turbines rotate at a relatively high frequency compared to large turbines. As pointed out in the rotor section, centrifugal forces are generally the largest design concern, even under normal conditions, but in the case of a blade failure a severe imbalance of the rotor may occur. This imbalance gives rise to an eccentric force in the rotating shaft because of the remaining blades. Since many small wind turbines may reach

high rotational speeds, centrifugal force can be several tons even for a turbine rated at 1kW, which can ultimately damage the generator shaft or the structure. Since the generator accounts for a significant part of the overall cost of the turbine, a damaged generator will generally lead to a total loss of the turbine.

Blade forces during extreme and turbulent wind events. Small turbines generally align themselves with the wind direction by means of passive yawing, so large and rapid changes in turbine orientation are common. Moreover, some wind turbines use furling mechanisms, which rotate the complete wind turbine abruptly and deviate it from the prevailing wind direction. These conditions induce gyroscopic forces in the blade root and the clamping supports. Those forces sum up with the aerodynamic bending moment; the gyroscopic forces are not axially symmetric because each blade experiences a particular force according to its angular position. This imbalance tries to bend the generator shaft and in extreme cases can lead to air-gap closure in the generator, the ultimate consequence of which is a magnet collision with the stator.

5. Control mechanisms

Control and protection mechanisms are peripheral elements that are necessary to ensure the reliability and long-term performance of a wind turbine. These mechanisms vary significantly with wind turbine size. While large turbines rely on active blade pitch and mechanical brakes, small wind turbines frequently use passive mechanism and controlled short circuits. The most common control mechanisms in small wind turbines are discussed below.

5.1 Furling systems

Furling is a passive mechanism used to limit the rotational frequency and the output power of small-scale wind turbine in strong winds. While other mechanisms, such as passive blade pitching or all-electronic control based on load-induced stall can occasionally be encountered, furling is the most frequently used mechanism. The basic idea is the turn the rotor out of the wind once a critical wind speed value has been reached. This principle is illustrated in Fig. 9 where photographs of an operating commercial wind turbine (Aeroluz Pro, rated at 1.4kW) are shown for normal operation (a) and under furled conditions (b).

Fig. 9. Furling mechanism operating in a commercial wind turbine rated at 1.4kW. (a) Normal (unfurled) operation. (b) Furled turbine.

The basic operating principle is sketched in Fig. 10. The mechanism is based on the interplay of three torques caused by the aerodynamic forces on the rotor and the tail vane, respectively, as well as a force of restitution, often provided by gravity in conjunction with an appropriate inclination of the tail axis. Due to an eccentric mounting of the turbine the axial force creates a moment around the vertical turbine axis, tending to turn the turbine out of the wind (counter-clockwise rotation in Fig. 10). At low or normal wind speeds this rotation is avoided by two opposing moments working in conjunction. Firstly, the aerodynamic torque on the tail vane tends to realign the vane with the wind direction, thereby causing a clock-wise rotation of the vane with respect to the generator structure. Now, if the tail rotation axis (generally referred to as the furl axis) is chosen not be non-perpendicular to the horizontal plane, then this rotation results in an increase in gravitational potential energy, which translates into an opposing torque for the turbine rotation. If the wind speed is strong enough, however, the opposing torques will be overcome and the turbine furls (Fig. 10 (b)). If the wind speed is reduced, then the moment of restitution prevails and operation of turbine in alignment with the wind direction is reestablished.

The transition into the furling regime and back to normal operation for a selected case is shown in Fig. 11, where both the yaw (a) and the furl angle (b) have been plotted as a function of the steady-state wind speed for (i) entering and (ii) exiting the furling regime.

These results were obtained by feeding a constant wind speed into a dynamic model of the furling mechanism of a small wind turbine (Audierne et al. 2010) and observing the

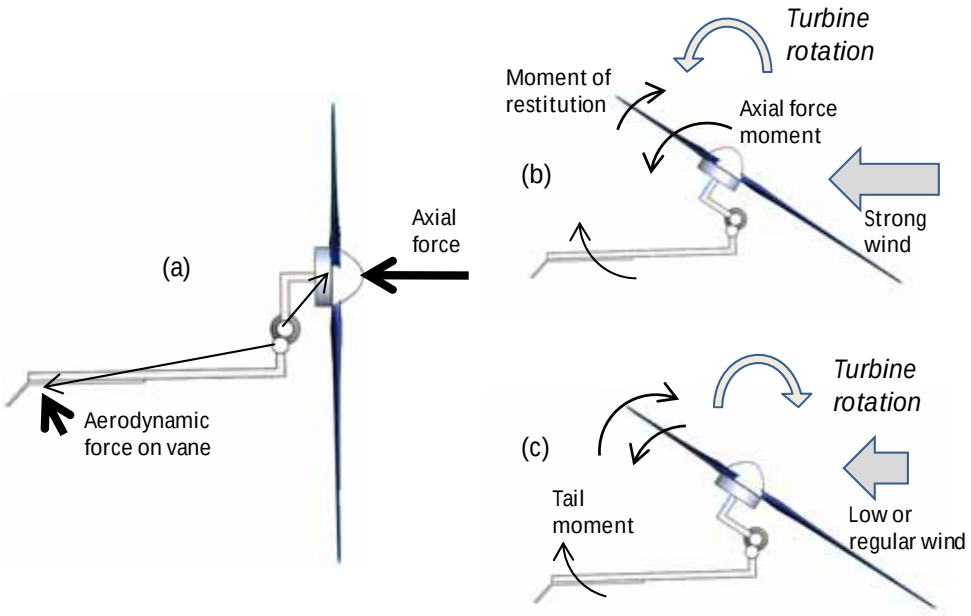

Fig. 10. Overview of the operating principles of a furling system. (a) Aerodynamic forces. (b) Furling movement in strong winds. (c) Restitution of normal (aligned) operation upon reduction of the wind speed.

asymptotic value of the yaw and furl angle, respectively. It can be seen from Fig. 11 that in this particular case the onset of furling, characterized by a steep transition of the angles, occurs at about 12.25 m/s. In order to return to normal operation the wind speed has to be lowered below that value, in this case to about 12.15 m/s, i.e. some hysteresis occurs.

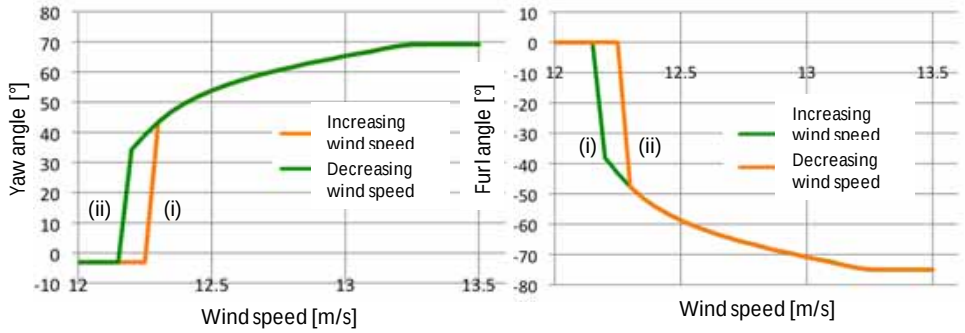

Fig. 11. Simulation results for steady state transition for (i) Entering, (ii) exiting the furling regime. (a) Yaw angle, (b) furl angle.

This hysteresis is quite common in furling mechanisms and can be traced back to the different variation of the torque components with the yaw angle. This allows the designer to fine-tune the system according to his or her requirements; see Audierne et al. (2010) for details. It should be noticed that in the case exhibited in Fig. 11 a relatively smooth transition to the asymptotic values of the angles occurs after the initial steep transition, allowing for a relatively smooth variation of the power curve beyond the onset of furling, as opposed to situations where the rotors jumps to its stop position (about 70° in this case) abruptly.

Due to this hysteresis it can be anticipated that that additional complexity will be present in the case of a dynamically varying wind speed. To explore this dynamics, stochastic wind speed time series (Amezcua et al., 2011) with a given turbulence intensity, a defined Kaimal turbulence spectrum and specified gust values was fed into the simulator developed for furling system (Etienne et al., 2010). 15 realizations of each stochastic process were simulated and the results of furling calculations for these 15 runs were averaged. An initial hypothesis was that short gusts beyond the steady-state wind speed for the onset of furling might trigger a transition into the furling regime where the system would be trapped due to hysteresis. In Fig. 12 a phase diagram identifying the system phases (non-furled, furled, transitioning) has been plotted for two cases of the standard deviation of the wind speed. The variable plotted on the horizontal axis is the mean wind speed of the time series, whereas the vertical axis shows the difference between the gust and the mean wind speed, i.e.

$$\Delta v = v_{\max} - \langle v \rangle = \langle v \rangle G \qquad (16)$$

where G is the gust factor. In the case of a low standard deviation of 1m/s (Fig. 12 (a)) a clear dividing line can be seen between the two main regimes, i.e. the normal operation regime with yaw angles of up to about 15°, and the furling regime, where the yaw angle is in excess of 60°. The transition between the two regimes occurs in a thin range around the dividing line the width of which is essentially constant for all ($\langle v \rangle$, Δv) combinations. It is intuitively clear that for smaller average wind speeds $\langle v \rangle$ the required gust Δv (measured relative to

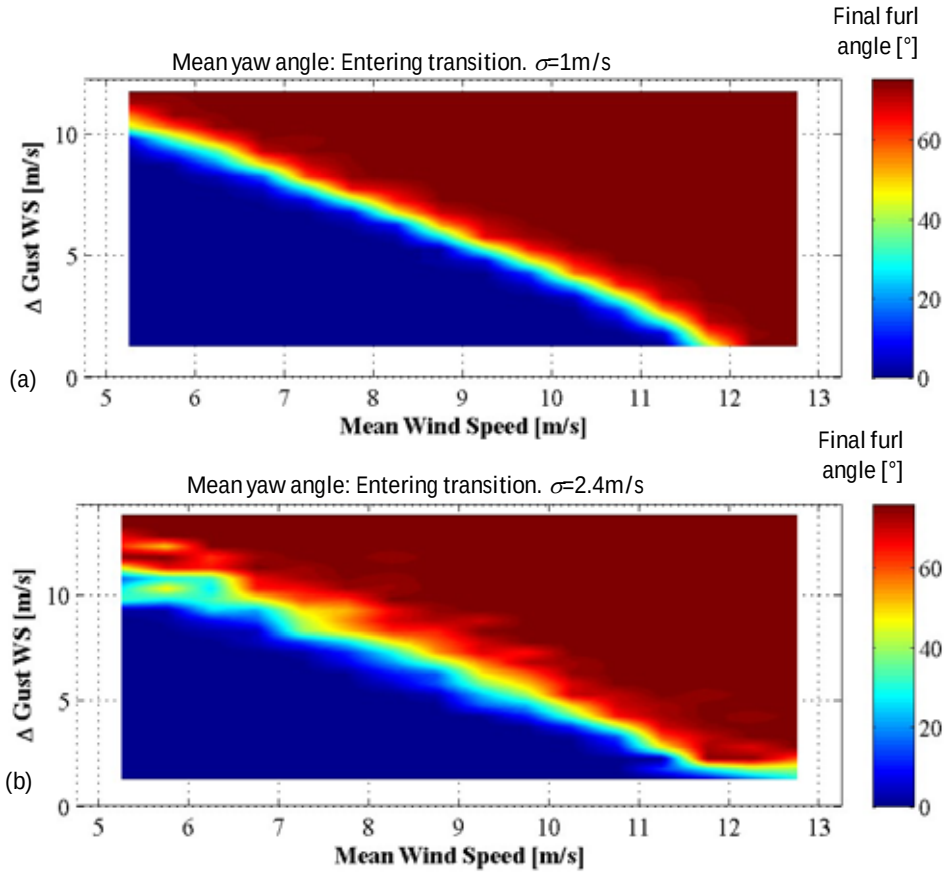

Fig. 12. Phase diagram for dynamic transitions into the furling regime: Simulated asymptotic value of the yaw angle as a function of the mean wind speed and the difference between the gust and the mean wind speed. a) Wind speed standard deviation = 1 m/s, b) standard deviation = 2.4 m/s.

the mean wind speed) for triggering a transition into furling has to be higher than at high wind speeds. As expected, for zeros gust (G=0) transition to furling occurs approximately at the critical steady-state wind speed (about 12 m/s in this example).
The fact that the transition boundary is approximately a straight line with negative slope can be stated in terms of the following simple equation

$$\alpha\ \Delta v + \langle v \rangle = \frac{\tau}{T}\ \Delta v + \langle v \rangle = v_{ss}\ , \tag{17}$$

Where T is the simulation time frame and τ the effective gust duration and v_{ss} is the steady-state wind speed value for the transition to furling. Using the graph in Fig. 12 (a) an effective relative gust duration $\tau\ /T$ can be estimated. While $\tau\ /T$ <1 in all cases simulated, the

effective gust duration determined this way is considerably larger than the real gust duration (typically 15s), indicating that a short gust that takes the total wind speed over the threshold value may be sufficient to trigger the transition to furling, even if the average wind speed in the interval is low. As mentioned earlier, the hysteresis between the transitions to and from the furling regime is a plausible qualitative explanation of this phenomenon.

Not unexpectedly, a higher turbulence intensity gives rise to a more stochastic behavior near the transition boundary, as shown in Fig. 12 (b), where the phase diagram in the $<v>$- Δv plane has been shown for a value of the standard deviation of 2.4m/s. While still the linear relationship between the critical $<v>$ and Δv values can be seen, the boundary is now blurred out, indicating a more chaotic movement of the rotor angle near the threshold. Interestingly, higher fluctuations can be seen for low mean wind speeds, where the turbulence intensity is higher than for high $<v>$ values, given the fact that the standard deviation and not the turbulence intensity was held constant in the simulations.

While more complex phase diagrams can be produced by choosing extreme value of the geometric parameters of the system, for plausible design parameters it can be seen that the system behavior remains relatively predictable (in a statistical sense), so that a stationary analysis provides a useful guidance for the design of furling systems.

5.2 Load-induced stall control

Stall control is a common practice in fixed rotational speed wind turbines and was used in utility-size turbines until relatively recently, when multi-megawatt turbines became the standard for commercial wind farms. Some utility-scale turbines, such as the NEG-Micon 1.5MW (later upgraded to 1.65MW under the label Vestas), also used active stall control, where the blade is pitch in the opposite direction as compared with regular pitch control.

In small wind turbines stall control had been used by different means, either by rotating the blade through a mechanism activated by centrifugal forces (Westling et al., 2007) or by changing the rotational speed. This last approach has the advantage of reducing the moving parts and hence increasing the reliability. Variations on rotational speed can be caused by changing the load on the generators terminals. If a smaller load is connected, higher current will be demanded and therefore higher mechanical torque. This will lead to a reduction in the rotational speed and higher angle of attack. Stalled blades will reduce output power of the wind turbine as shown in Fig. 13 (Elizondo 2007). These results were obtained with an experimental wind turbine built based on a Bergey XL.1 commercial wind turbine generator, but equipped with a specially designed rotor and tail vane (Elizondo, 2007). A simple load control was implemented based on a switchable resistor bank, where the value of the load was changed as a function of the measured wind speed.

For wind speeds from 0 to 6.0m/s the load was a resistance of 3Ω, which was reduced to 1 Ω at 6.1m/s, 0.3 Ω at 7.1m/s, and 0.25 Ω at 8.1m/s. Without the intervention of the control system (i.e. for a constant load of 3 Ω) the system would be expected to operate in near-optimal conditions for wind speeds of up to about 7m/s; consequently, power should increase as the cube of the wind speed. Due to the change in load from 3 Ω to 1 Ω at 6.1m/s power increases a little slower, but the change is not obvious from the graph. Actually, instead of operating at a tip speed ratio (TSR) slightly above the TSR for optimum system power coefficient $C_{p,system}$ at a wind speed of 7m/s, due to the change of load the system now operates under mild stall conditions with a slightly lower $C_{p,system}$. The difference

becomes more conspicuous at higher wind speeds of about 7 to 8m/s where a clear change of curvature in the P(v)-curve is apparent. When the resistance is lowered to 0.3 Ω at 8.1m/s, a noticeable change occurs, with a clear reduction in slope of the P(v) curve, leading to a plateau of the power production. At a wind speed of 9.1m/s a further reduction of load to 0.25Ω is induced by control system, but this small increase in load is incapable of coping with the increase of available power density; consequently, power production increases again. It should be noted that this behavior is a specific limitation of the Bergey XL.1 generator which was designed to operate with a different control system and whose intrinsic (armature) resistance is too large to allow for a further reduction of the load resistance, as required for a full-scale active-stall control.

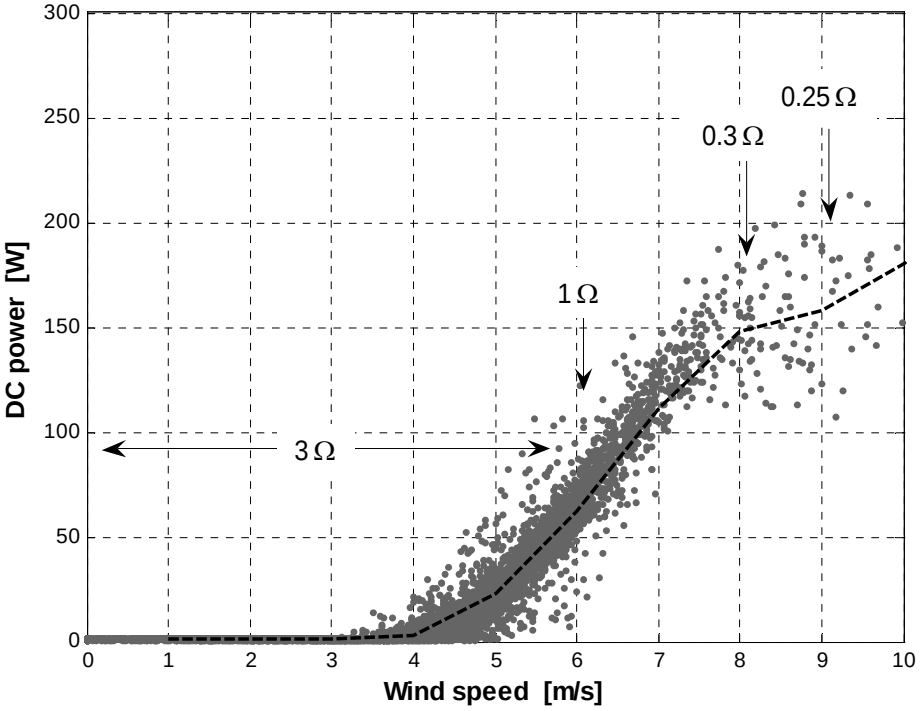

Fig. 13. Proof-of-concept demonstration of active stall regulation

5.3 Passive blade pitch

Blade pitching is very common among mega-watt size wind turbines where a motor is used to rotate the blade along its axis depending on measured wind speed and desired performance. This principle has also been used in small wind turbines but usually with passive mechanisms that convert an existing force into the blade rotation.

Mechanisms vary significantly depending on the manufacturer and the purpose of the pitch. Some turbines use the pitch mechanism as a means of power control, however, since the system is passive, a precise control is hard to achieve and therefore most turbines just implement it as a protection system against high wind speed or high blade rotational speed.

In any case, the operational principle is to reduce the accelerating wind force on the blades, by changing the angle of attack in the airfoil sections. Examples of blade rotations both to increase angle of attack and reach stall conditions (pitch to stall), or to decrease angle of attack (pitch to feather) can be encountered in commercial wind turbines. The activation of the mechanism commonly uses the centrifugal force, where the radial movement of the blades induces the rotation. However, in some cases the aerodynamic torque caused by pressure difference along the airfoil chord has also been used. Restoration of the unpitched blade orientation is usually achieved using springs attached to the blades that overcome the activation force when non-operational conditions finish. In principle, any other force such as gravity may be used to restore the blade orientation.
One critical aspect to consider when implementing a passive blade pitch system is to ensure that all blades rotate at the same time in order to prevent aerodynamic or inertial imbalance that may damage components of the wind turbine. Furthermore, a careful balance between the activation and restoration force of the mechanism has to be considered in order to avoid system oscillations that will cause damage in the long-tem.

6. System behavior

6.1 Power flows and efficiency

In general terms, power losses in small-scale wind systems are significant, given the fact that small wind turbines generally operate at low voltages; this is particularly notorious in battery-charging systems where typical system voltages are in the range of 12V to 48V. The different loss mechanisms cover a quite wide range for each loss component, given the range of electric power and rotational frequencies encountered. At low frequencies, rotational friction at the shaft bearings is the dominant loss mechanism, where at nominal output power normally Joules losses in coils and cables play the most important role. Generally, the point of maximum efficiency does not occur at maximum output power due to the interplay between the extraction of aerodynamic power (peaking at a given rotational frequency for a given wind speed) and the losses of power in the electromechanical system (which generally increase with rotational power).
An overview of the power conversion stages occurring in a small wind system, together with the main loss mechanisms is given in Fig. 14. The power delivered to the rotor-generator shaft by the extraction of power from the wind is first transformed into electromagnetic power, with losses corresponding mainly to friction at the bearings and ventilation losses. In order to produce power at the generator terminals, energy has to be converted at the generator, involving Joule losses at the armature resistances of the stator coils, eddy losses in coils, as well as losses at the ferromagnetic core, if present. Joule losses at the coils are generally the dominant loss mechanism at small wind turbine generators, especially at higher power values. If an electronic converter is used, such as for maximum power point tracking and related functions, then additional losses occur at this stage, although these losses are generally more than compensated by the corresponding gain in aerodynamic efficiency of the rotor. Before getting to the load, a transmission line is required. Even if the load is placed at the foot of the tower (an unlikely situation), the minimum length of the line is still of the order of 20m to 30m, generating substantial losses if the power is transmitted in 12V or 24V. While self transformers can in principle be used to raise the level of the transmission voltage, the compact size of the nacelles of small wind turbines often does not allow for such a measure. Moreover, the system complexity

increases by requiring a second transformer near the load in order to return to the system voltage. In the case of battery-charging systems, the rectifier has to be placed after the second transformer, so the whole transmission line has to be three-phase, which increases the system cost beyond the additional expenses for the transformers. After delivering the power to the load, there are still losses occurring at the cabling of the load, as well as internal losses, so selecting an efficient end-use device is important to obtain an efficient overall energy service.

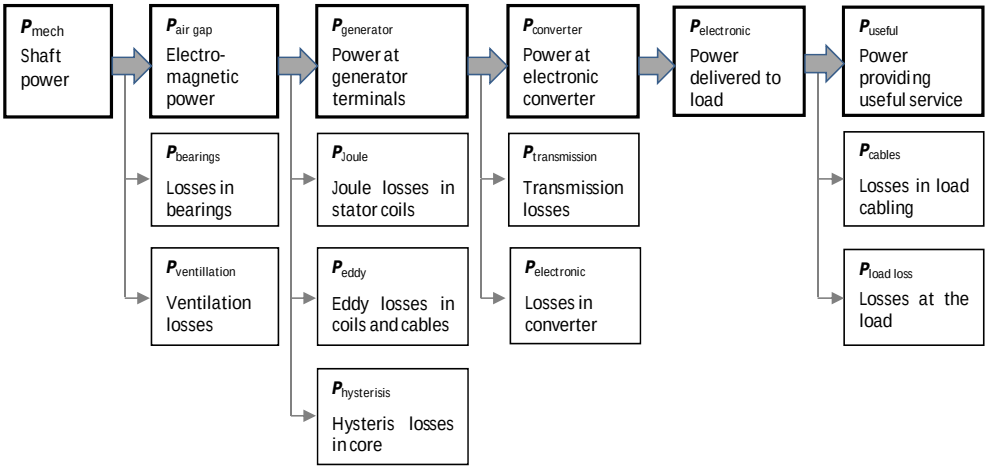

Fig. 14. Power conversion chain at a small wind system. The upper chain identifies the main conversion stages, while the lower boxes describe the losses occurring at each stage.

Typical component efficiencies are the following: (1) Generator efficiencies may vary widely, depending on the design, the manufacturing accuracies, and the operating point. Commercial generators generally have efficiencies of 90% and beyond, while the efficiency of home-built generators may be as low as 65%. Similar efficiencies (65%-95%) apply for the transmission line, where higher transmission voltage (such as 48V) helps keeping the losses at an acceptable level. The downside of a 48V system voltage is the fact that few appliances are available for this voltage level, as opposed to 12V where an abundance of products exists due to the use of this system voltage in the automotive sector. The efficiency for delivering power to the load is in the range of 60% to 85% if a battery bank and a subsequent DC/AC converter is used.

The total system efficiency, based on these values, is in the range of 25% to 75% if batteries are used for energy storage, and 45% to 85% for grid-connected systems. From the discussion above it is clear that a high-quality electric system and installation are essential. This is particularly true in small systems with a rated output power of 1kW or less, and even more so in home-built systems where the overall available power may be deceptively low and hardly enough to light a few light bulbs.

6.2 Steady-state system behavior

In order to determine the steady-state operating point of the wind system it is necessary to specify two variables on both ends of the generator: (1) On the upstream side either the shaft

frequency or the mechanical torque can be specified. (2) Possible variables on the downstream side include the output voltage or the electric current. A useful tool in the design of the system operation is a diagram where the power supply and demand curves are shown as a function of the rotational frequency *n* (Fig. 15).

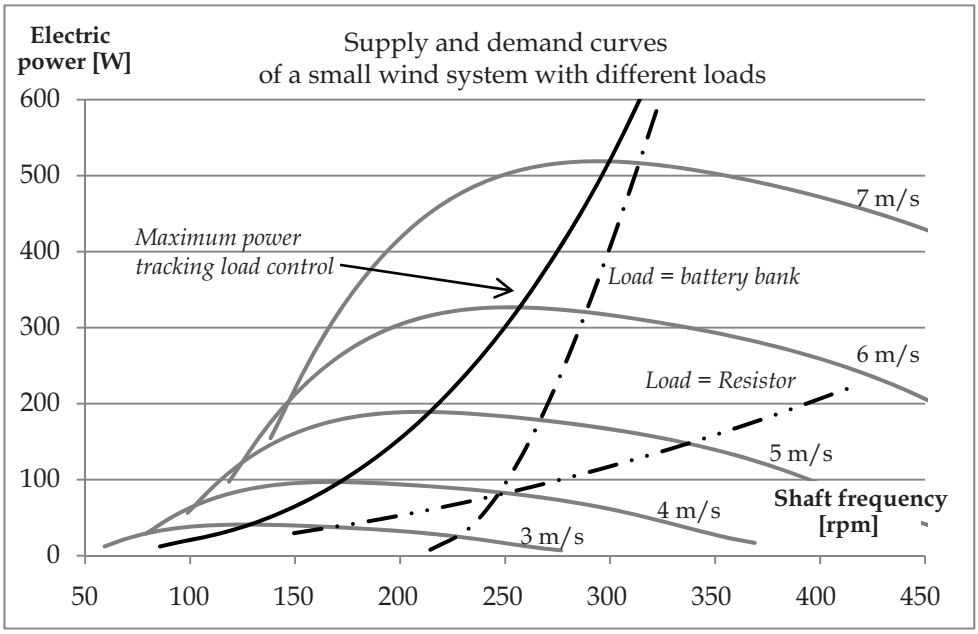

Fig. 15. Supply and demand curves for different wind speeds and load types.

In Fig. 15 the supply curves (converted into electric power curves by incorporating all inefficiencies and their respective dependencies on *n* in the conversion from shaft to load power) have been drawn for a wind turbine with a swept diameter of 3.0 m for different wind speeds in the range of 3 m/s to 7 m/s, together with the load curves for (a) a simple fixed electric resistor (such as a light bulb), (b) a battery bank, and (c) a load equipped with an electronic load control, in this case designed to track the maximum electric power point. It can be seen that an electric resistor generally represents a load which is inappropriately matched to the source, since only at certain wind speeds an operation close to optimal conditions is possible, even for the relatively broad supply curves shown in this example. Clearly, a direct connection of the wind turbine to a resistor is not an efficient means of utilizing the power extracted from the wind and will not be used in other than the simplest systems. One possible example is electric space heating in cold climates with strong winds where an abundance of the wind resource may minimize concerns about overall efficiency. Under these conditions, also the fluctuating nature of the wind resource which directly translates into a fluctuating output power is of less importance, since the heated space itself acts as a storage medium.

If a battery bank is used as a load, the source-load match improves substantially. If the supply curves and the system voltage are appropriately matched, a certain self-regulation occurs in this case, since the power draw from the battery matches the supply from the

rotor-generator quite well for all wind speed values other than the very low ones. The poor match at low wind speeds is due to the simple fact the a minimum rotational speed is required for a synchronous generator in order to produce at least the battery voltage at its terminals, so no charging (and the corresponding power flow) will occur at shaft frequencies below the critical value. Battery-charging systems are quite common for remote electrification, and a direct connection of the wind turbine to the battery bank may be a viable alternative for cost-sensitive applications.

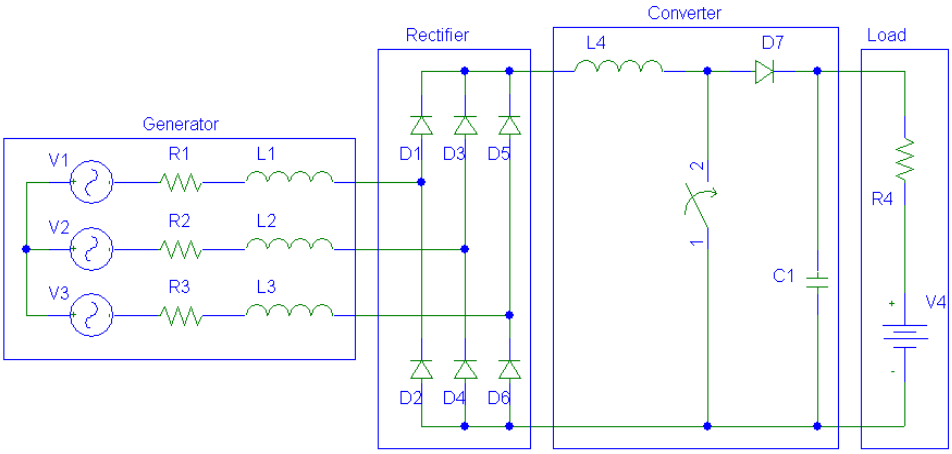

Fig. 16. Simple boost controller operating with a three-phase generator and rectifier, as well as a battery bank.

In the case of grid-connected applications where a reduction of the electric bill is the main concern, a load control to ensure an optimal extraction of the available wind power may be appropriate. As shown in Fig. 15 a maximum power point tracking load may significantly increase the output power at low wind speeds and improve the starting behavior of the turbine. As mentioned in the preceding paragraph on battery charging, the problem to be overcome at low rotational frequencies (required to match the supply curves at low wind speeds) is the low voltage produced by the generator under these conditions. An electronic device which dynamically changes the apparent load impedance can solve this problem. A simple scheme designed to boost the voltage is shown in Fig. 16 where a three-phase generator, operating with a passive six-pulse rectifier, is connected to a battery bank through a switching device. The switch can be a Mosfet or an IGBT device and is fed by a pulse width modulated (PWM) signal generated by a control unit, often a micro-controller. Opening and closing the switch generates a modulated current and therefore an induction voltage at the inductor which is smoothed out by the capacitor. The average output voltage can be adjusted by varying the duty cycle of the switching process. The inductor shown in Fig. 16 is often not necessary, since the self inductance of the generator can be used for that purpose.

This simple device can be used in different ways to control the operation of the small-scale wind system: (1) As mentioned before, boosting the voltage at low wind speeds allows charging of the battery bank at wind speeds well below the critical value for constant load

voltage. (2) At high wind speeds the current can be increased in order to operate the turbine under partially stalled conditions and slow down the rotor. This is a convenient way of controlling the operation of the turbine at high wind speeds. If appropriately designed, the rotor will dissipate most of the excess power available at high wind speeds by entering the stall regime, limiting the electric power dissipation in the generator due to the increased current.

6.3 Mathematical modeling

Despite their apparent simplicity, small-scale wind turbines are complex systems. This makes it necessary to establish a mathematical model which couples all the physical processes occurring in the system and can provide accurate guidance during the design, analysis, and continuous improvement. A good starting point is a conceptual model of the electric generator which can be used to identify all the physical processes and develop a more detailed model of the magnetic flow topology, the effective electric parameters and the heat transfer. Often, the electric load characteristics can be studied in a lumped circuit model, but the values of the effective parameters such as armature resistance and stator inductance have to be determined from the more detailed model, if the costly construction of a series of prototypes for measurement and optimization purposes is to be avoided. Detailed mathematical models have been developed for certain generator topologies (see, e.g., Bumby et al., 2005; Gieras et al., 2008), but numerical multi-physics models can also be conveniently constructed with tools like Comsol (see examples in section 5).

Once the generator characteristics are sufficiently well known, effective load curves can be constructed for typical situations, such as a battery or a resistive load. Also, the total generator efficiency (including the rectifier if a DC application is sought) as a function of the rotational frequency should be known in order to narrow the range of the steady-state operating points, the exact location of which will of course depend on the detailed rotor characteristics. The rotor is generally modeled using Blade Element Momentum theory with suitable expressions for the aerodynamic lift and drag coefficients, as discussed earlier. As it was mentioned before, the available wind speed and the instantaneous electrical load connected are the principal factors determining the operating point of the generator. For most purposes, a steady-state operating model of the turbine will be enough, although the assessment of failures will generally require a transient model of the system, as discussed in section 5. A control model which appropriately maps the aerodynamic mechanisms such as furling or passive pitching and the electronic control elements such as load control (if present) will conclude the analysis of the operating characteristics of the wind turbine.

Thermal characteristics finally, such as the heat transfer mechanisms, are important to know in order to define the generator's loading characteristics. A proper thermal design should also the consider the ventilation properties of the rotor-generator, since a wind turbine has some intrinsic thermal self-regulation characteristics, given the fact that high wind situations, where efficient cooling by forced convection is available, generally correlate with high power output.

The results of the modeling process can be conveniently summarized by a performance map, defined as a set of tables showing the values of the different variables of interest as a function of both the wind speed and the rotational frequency of the generator. Variables of interest include the electric output power, the temperature of the stator coils, the terminal voltage and the electric current. The information of the different tables can be combined by marking table cells where critical conditions for any of the variables occur. The performance

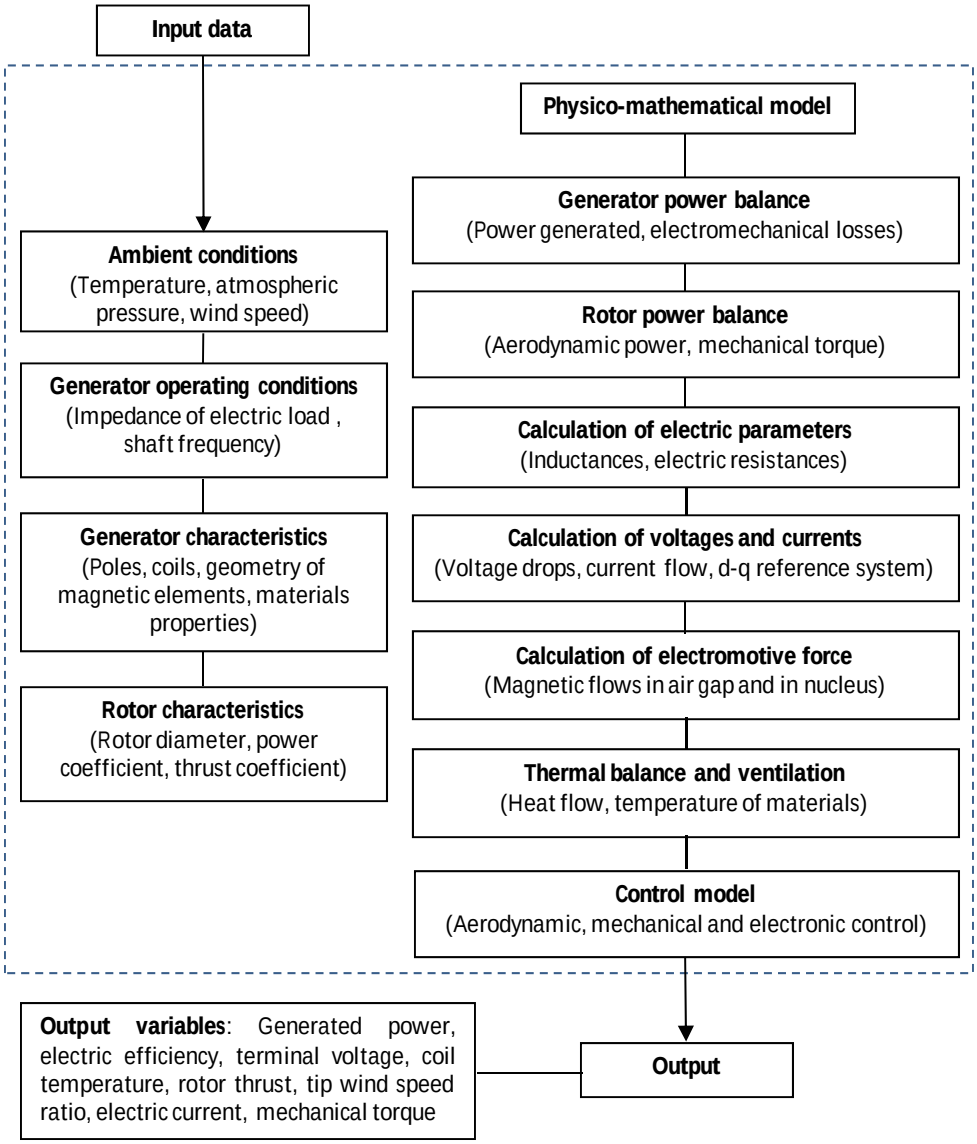

Fig. 17. Schematic representation of the system modeling process

map can then be used to establish operating limits, desirable operation points or zones, and methods of regulation, control, and protection. In Table 2 an example of such a performance map (shown for the variable output power) for a small wind turbine rated at 1.4 kW.

	U_{wind} (m/s)					
	4	6	8	10	12	14
n (rpm)	P_{gen} (W)					
50	4	7	10	14	19	24
100	55	54	54	63	71	82
150	**84**	186	200	177	186	204
200	78	281	417	457	437	429
250	52	312	606	735	768	777
300	16	**313**	714	1,009	1,021	**940**
350	0	291	775	1,239	**1,251**	**723**
400	0	249	**786**	**1,405**	1,615	**86**

Table 2. Performance map for a wind turbine rated at 1.4 kW. Dark-shaded cells: Optimal output power. Light-shaded cells: Regulated high-wind speed path. Hatched cells: Overheating coils.

At low wind speeds reaching the maximum output power point is desirable in order to make an efficient use of the relatively small available power density. For wind speeds of up to 8 m/s the required rotational frequency remains within a window where centrifugal forces on the blades are tolerable on structural grounds and noise due to air-cutting blades is not a serious problem. At still higher wind speeds, following the maximum output power point would lead to very high shaft frequencies and produce excessive heating of the stator coils. Therefore, limiting the rotor frequency by an appropriate control scheme is necessary. In the present example, limiting the rotor frequency to 400rpm, 350rpm, and 300rpm at 10m/s, 12m/s, and 14m/s, respectively, leads to a path where all system variables of interest remains within their allowed boundaries. Such a frequency control may be achieved using electronic load control, e.g. by actively inducing stall at (part of) the blades, by passively veering the rotor out of the wind (furling, see section 4), by passively pitching the rotor blades, or a combination of the former. The vertically hatched cells in Table 2 correspond to situations where overheating of the coils occur (due to high dissipation due to Joule losses and others) and have to be avoided.

7. Summary and conclusions

Small-scale wind turbines are an attractive option for a host of remote applications, such as rural electrification, water pumping or telecommunication, and also provide an option for saving energy and mitigating greenhouse gases in grid-tied situations. While conceptually simple, small wind turbines are quite complex systems and require a professional design,

construction and operation. While motivated individuals with a sufficient engineering background may be capable of designing and building a functional wind turbine, its performance may be deceptively low, unless great care is taken to design, construct and operate the system based on best engineering practice. As pointed out above, the rotor design and performance evaluation have specific issues related to low Reynolds number flow and 3D aerodynamic effects. The generator, on the other hand, in general has to be designed for a given application, which precludes the use of off-the-shelf appliances in most cases, unless suboptimal operation is tolerable. Manufacturing of the generator is critical due to the small gap widths required for efficient magnetic flow, and potentially hazardous events have to be considered early in the design stage. The control mechanisms, finally, are key to the efficient operation of the turbine under normal operation and will keep the turbine safe in extreme winds. And last, but certainly not least, design for safety should guide the whole process, and certification of the performance and safety characteristics (e.g. according to AWEA (2009)) should be obtained for any turbine intended for commercial sales.

8. References

Amezcua, J.; Muñoz, R.; Probst, O. (2011). Reconstruction of gusty wind speed time series from autonomous data logger records, *Wind & Structures* (accepted)

Audierne, E.; Elizondo, J.; Bergami, L.; Ibarra, H.; Probst, O. (2010). Analysis of the furling behavior of small wind turbines, *Applied Energy* 87(7): 2278-2292

AWEA Small Wind Turbine Performance and Safety Standard AWEA Standard AWEA 9.1 – 2009. Available at http://www.smallwindcertification.org/.

Bang, D.; Polinder, H.; Shrestha, G.; Ferreira, J.A. (2008). Review of Generator Systems for Direct-Drive Wind Turbines. Proceedings of the European Wind Energy Conference (EWEC) 2008.

Baroudi, Jamal A.; Dinavahi, Venkata; Knight, Andrew M. A review of power converter topologies for wind generators. University of Alberta, Edmonton, AB, Canada, 2007

Bumby, J.R.; Martin, R. Axial-flux permanent-magnet air-cored generator for small-scale wind turbines. IEE Proc. Electr. Power Appl., Vol. 152, No. 5, September 2005

Burton, T.; Sharpe, D.; Jenkins, N., Bossanyi, E. (2001). *Wind Energy Handbook*, John Wiley & Sons

Dubois, M.R.; Polinder, H. Ferreira. J.A. (2000) Comparison of generator topologies for direct-drive wind turbines. Delft University of Technology 2000.

Elizondo, J. (2007). Diseño, manufactura y caracterización experimental de aspas y controlador de carga resistiva para una turbina de viento Bergey BWC XL.1. Master Thesis, Instituto Tecnológico y de Estudios Superiores de Monterrey, Monterrey, Mexico (in Spanish)

Elizondo, J.; Martínez, J.; Probst, O. (2009). Experimental study of a small wind turbine for low- and medium-wind regimes. *International Journal of Energy Research* 33:309–326, John Wiley & Sons, Ltd

Gieras, Jacek F. Performance Characteristics of a Permanent Magnet Transverse Flux Generator. IEEE, 2005

Gieras, Jacek F.; Wang, Rong-Jie; Kamper, Maarten J. Axial Flux Permanent Magnet Brushless Machines. 2nd Edition, Springer 2008

Khan, M.A.; Pillay, P.; Visser, K.D. (2005). On Adapting a Small PM Wind Generator for a Multiblade, High Solidity Wind Turbine. IEEE Transactions on Energy Conversion Vol. 20, No. 3, 685-692

Kutz, M. (2005). Handbook of Environmental Degradation of Materials. William Andrew Publishing.

McGhee, R.J., Walker, B.S., and Millard, B.F. (1988). Experimental Results for the Eppler 387 Airfoil at Low Reynolds Numbers in the Langley Low-Turbulence Pressure Tunnel. NASA TM 4062

Martínez, J.; Morales, A.; Probst, O., Llamas, A., Rodríguez, C. (2006). Analysis and simulation of a wind-electric battery charging system. *International Journal of Energy Research* 30:633-646 John Wiley & Sons, Ltd

Martínez, J.; Bernabini, L.; Probst, O; Rodríguez, C. (2005). An improved BEM model for the power curve prediction of stall-regulated wind turbines. *Wind Energy*, vol. 8, pp. 385-402, John Wiley & Sons, Ltd

Probst O., González A., Roidl M., Llamas A. (2006). A small wind–electric system based on an improved version of the ITDG axial flux permanent magnet generator. *Wind Engineering* 2006; 30(5):385–400.

Wastling, M.A; Balson, J.Ch.; Irving, D.; Cann, R.J. (2007). United States Patent US 7,172,392 B2

Yicheng Chen; Pragasen Pillay; Khan, A.. (2004) PM Wind Generator Comparison of Different Topologies. Industry Applications Conference, 2004. 39th IAS Annual Meeting. Conference Record of the 2004 IEEE

Yicheng Chen; Pillay, P.; Khan, A.; PM wind generator topologies. IEEE Transactions on Industry Applications 2005; 41:1619-1626

Selig, M.S., McGranahan, B.D. (2004). Wind Tunnel Aerodynamic Tests of Six Airfoils for Use on Small Wind Turbines. NREL/SR-500-34515. National Renewable Energy Laboratory, Golden, Colorado, USA

Somers, D.M., Maughmer, M.D. (2003). Theoretical Aerodynamic Analyses of Six Airfoils for Use on Small Wind Turbines. NREL/SR-500-33295. National Renewable Energy Laboratory, Golden, Colorado, USA